Journal of Social Sciences and Technical Education, 4(1), 113-126
http://myjms.mohe.gov.my/index.php/jossted

Design and Development of A Low-Cost Electromyogram Amplifier for General-Purpose Biosignal Amplification

(Rekabentuk dan Pembangunan Penguat Elektromyogram Kos Rendah Bagi Amplifikasi Isyarat-bio Umum)

ZINVI FU[1*], AHMAD YUSAIRI BANI HASHIM[2], ZAMBERI JAMALUDIN[3], IMRAN SYAKIR MOHAMAD[4]
Department of Mechanical Engineering, Politeknik Ibrahmin Sultan, Malaysia[1*]
Faculty of Manufacturing Engineering, Universiti Teknikal Malaysia Melaka, Melaka, Malaysia[2,3]
Faculty of Mechanical Engineering, Universiti Teknikal Malaysia Melaka, Melaka, Malaysia[4]

* Corresponding author: zinvifu@pis.edu.my

ARTICLE INFO

Article History:
Received 29.05.2023
Accepted 13.06.2023
Published 23.11.2023

Abstract

The electromyogram (EMG) is a biological signal which manifests during muscle contraction. It is widely used for health, biomechanics and machine control. However, high-performance EMG amplifiers are costly while self-developed solutions face reliability issues. In this paper, a low-cost solution to EMG amplification is introduced. The proposed design incorporates a front-end filter, a differential stage, and a bandpass filter. The resulting prototype consists of six differential inputs and is constructed into a compact housing. Being battery-powered, it is portable and safer as it is not powered by the mains. The developed device was rated to achieve a common-mode rejection ratio (CMRR) of over 90 DB with a high input impedance of 20 GΩ which is comparable to the commercial device. In addition, test results also showed that the baseline noise amplitude was similar with or without the right-leg drive.

Keywords: Electromyography, filter design, analogue amplifier, bio-amplifier

INTRODUCTION

The electromyogram (EMG) is a biological electric signal that manifests around the muscle when a contraction is performed. Muscle contraction continues if the EMG exists around the muscle. Since the EMG signal directly relates to body movement, the EMG signals can be harvested with electrodes, and the corresponding signals can be used by a machine to replicate the n motion (Yung & Wells, 2013).

While the EMG is widely applied in healthcare for diagnosing neuro-muscular conditions (Park et al., 2012) and designing prosthetic equipment (Hargrove et al., 2013), it is also accepted as a viable alternative to machine control interfaces. Owing to its advantages, EMG has been studied as the control signal for variants of machine interface, including human-computer interface (HCI), human-machine interaction (HMI) and human-robot interface (HRI).

EMG-based techniques are capable of accurately distinguishing natural human motion such as subtle finger movements and wrist motions by directly sensing and decoding muscular activity (Zhang et al., 2018). Since these signals are produced just before limb movement; therefore, they can be used to predict human motion intent and offer a higher degree of safety than physical signals (Artemiadis, 2012). In addition, EMG signals also carry information about the state of the body, such as muscle contraction level, stiffness, fatigue, and contraction speed, and can provide multiple observation indices for human-robot interaction (Rechy-Ramirez & Hu, 2015). Due to these properties, various EMG devices have found applications in portable/wearable equipment fitted closely to the human body and also for interaction and auxiliary control of remote systems (Ajoudani et al., 2012).

OVERVIEW OF EMG ACQUISITION

The harvesting of EMG signals begins at the skin level. Typically, electrochemical electrodes are used to couple the electric potentials on the skin to copper wires that connect to the signal conditioning and amplification stage.

When the electrode is connected to the skin, the cell circuit is complete allowing the current to flow into the amplification stage. A bipotential setup, as shown in Figure 1 provides the basis of modern bio-signal amplifiers (Northrop, 2001). The differential amplifier (DA) rejects the common-mode voltages while amplifying the EMG signal amplified. The resulting output signal is defined as Vo = Vi-Vi'.

In some designs, the right-leg drive (RLD) feedback loop is used instead. This addition further improves the CMRR, but also presents some stability issues (Alnasser, 2014). The impedance on the skin-electrode interface, Z_{skin} and the electrode-amplifier stage, Zelectrode should match to eliminate the common mode voltage (Jones, 2015). The DA with an input buffer stage allows impedance matching and forms an instrumentation amplifier, which is more commonly used in EMG circuits.

The following filter stage is responsible for removing unwanted signals at the extreme ends of the frequency spectrum. The offending noises usually are low-frequency movement artefacts, high-frequency electromagnetic radiation (EMI) and 50/60 Hz power line interference (PLI). Filtering is usually done with a bandpass filter of 10 -1000 Hz, and a 50/60 Hz notch filter. Filtering can be done with hardware (Wang et al., 2013) and software (Malboubi et al., 2010).

A wide range of EMG acquisition equipment from various manufacturers is commercially available in specifications to suit medical (Noraxon, Delsys) or consumer (Myo)

applications. Nevertheless, customized designs are continuously introduced in recent works as the commercialized devices may not be accessible or unsuitable for the works. Benatti et al. (2015), Tomasini et al. (2016) and Meattini et al. (2018) introduced an ARM-based embedded amplifier aimed at a high-performance portable EMG amplifier to the consumer-grade Myo. Their design incorporated a real-time SVM classifier which Myo lacks. (2008) proposed the design of a low-cost single amplifier with an SVM classifier that is efficient and can train in 30 s. Yoo et al. (2019) developed an Arduino-based cost-effective six-channel amplifier that provided output quality comparable to commercial systems. Avila et al. (2020) proposed a higher-density 16-channel amplifier with built-in electrodes already configured to SENIAM recommendations.

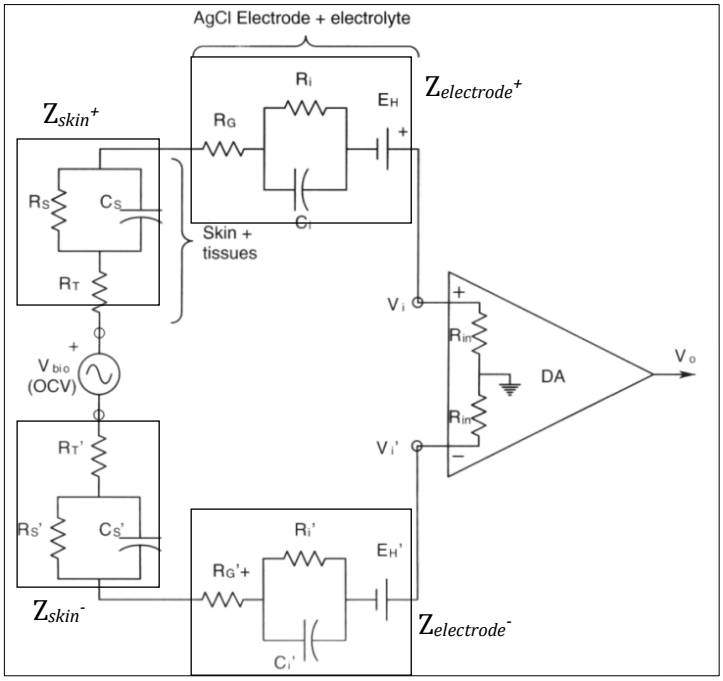

Figure 1. Equivalent circuit of the electrode in bipotential mode when connected to the skin and amplification stage (Source: Northrop, 2001)

PROBLEM STATEMENT AND OBJECTIVE

Commercial-grade EMG amplifiers are expensive and generally beyond the means of the independent researcher. For instance, full-featured multi-channel systems from Noraxon can cost RM10,000 upwards while single-channel amplifiers (e.g., Motion Labs Z03) can cost above RM1000 per channel. On the other hand, low-cost systems from various manufacturers such as Myoware and Groove cost between RM100 – RM300. However, these classes of system typically provide only integrated (amplitude level) outputs, which are more suited for basic machine control and may be unsuitable for temporal and frequency-based EMG analysis. On the other end of the spectrum, the basic components of the EMG amplifier are commonly available. Today, instrumentation amplifiers, operational amplifiers and high-precision discreet components can be purchased at a reasonable price, thus the EMG amplifier can be built and customized at a desired cost. However, custom-made EMG amplifiers normally suffer from low performance, particularly in the common-mode rejection ratio (CMRR), which is caused by the differential input impedance mismatch, inadequate shielding, filtering, or signal oscillation due to circuit instability.

In this work, the focus is on improving the CMRR by introducing a front-end filter to the common EMG amplifier design. The objective of this work is to propose a design which is low-cost while being able to provide an acceptable CMRR of above 90 dB. Apart from the

circuit design, validation also includes baseline measurement with or without the right-leg drive, and simulation and measurement of the input impedance and CMRR.

METHODOLOGY

The research process is divided into the circuit design, followed by the RLD test, input impedance simulation and CMRR measurement. The proposed design is then benchmarked against a commercial-grade EMG amplifier (Motionlabs Z03).

CIRCUIT DESIGN

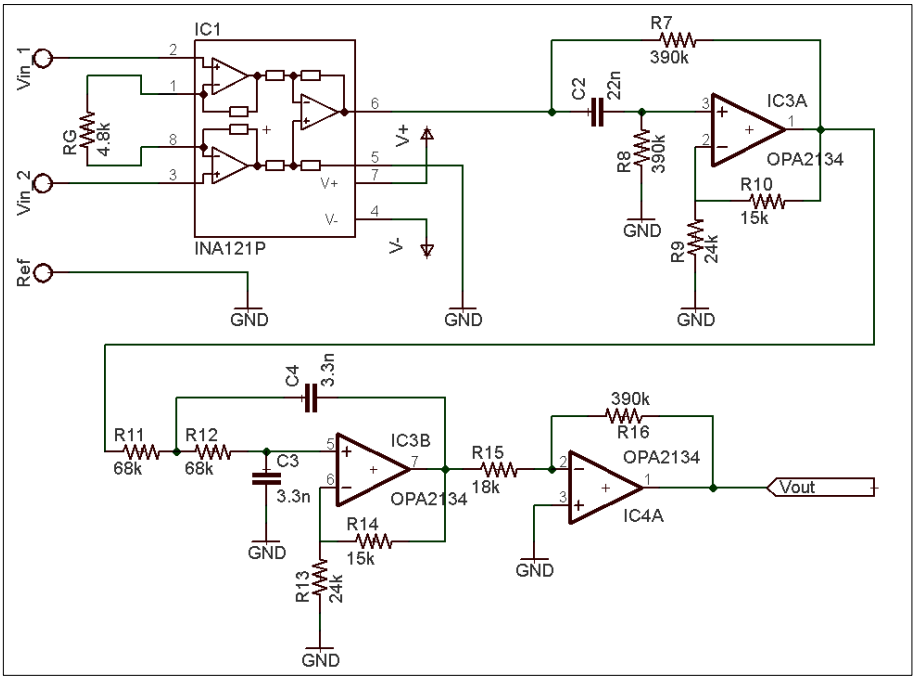

Figure 2. Schematics of EMG amplifier built with an instrumentation amplifier

The proposed EMG amplifier is shown in Figure 2. The EMG amplifier is built with the INA121P (IC1) instrumentation amplifier as the main unit. The inputs V_{in1} and V_{in2} provide the inverting and non-inverting differential input. This is followed by two second-order Sallen-Key active filters with op-amps, IC3A (high-pass filter) and IC3B (low-pass filter). Another op-amp, IC4A which is configured in non-inverting mode provides an additional adjustable gain.

The corner frequency, passband gain and Q factor of the second-order Sallen-Key filters are given in (1), (2) and (3) respectively. Based on the resistor and capacitor values in the schematics, the corner frequency, passband gain and Q factor for the filter stage are computed in Table 1. Since the energy spectrum of the EMG signal is between 20 to 500 Hz, the bandpass region of the design is adequate. The gain value was set as such to obtain a Q factor between 0.7 to 1.0 to achieve the steepest roll-off possible. Keeping a higher Q factor in conjunction with a gain greater than one can also reduce circuit noise (Steffes, 2012).

$$f_c = \frac{1}{2\pi\sqrt{R_1 R_2 C_1 C_2}} \quad (1)$$

$$G_{pass} = 1 + \frac{R_4}{R_3} \quad (2)$$

$$Q = \frac{1}{\sqrt{\frac{R_1 C_1}{R_2 C_2}} + \sqrt{\frac{R_1 C_2}{R_2 C_1}} + (1-k)\sqrt{\frac{R_2 C_2}{R_1 C_1}}} \quad (3)$$

Table 1. Filter design parameters of the bandpass filter

	HPF	LPF
Corner frequency, f_c	18.97Hz	709Hz
Passband gain, K	1.625	1.625
Q factor, Q	0.727	0.727

INPUT FILTER CONSIDERATION

In a biopotential recording, the main obstacle towards clean signals is the common-mode (CM) signal. Acquisition circuits will have to extract in the region of millivolts (ECG, EMG) and microvolts (EEG) from a CM signal of up to 1 V. There are many advanced methods to achieve a good signal-to-noise (SNR) ratio. Measurement systems that offer good SNR are due to the many filtering stages and adaptive correction (Staudenmann et al., 2006, Kim et al., 2011), and even customised signal processing devices. Other research optimized the performance of the fundamental circuit by improving the composition of basic components (Spinelli et al., 2003, Wang, 2013).

The heart of the biopotential amplifier is the instrumentation amplifier (INA) is a proven effective device for the job. It operates by a differential principle across two points, P_1 and P_2, giving (4)

$$V_{out} = K(V_{in1} - V_{in2}). \quad (4)$$

The difference at the input is here amplified by a gain of K. In reality, the input signal, V_{in} is defined as a collection of the EMG signal, V_{EMG} and the CM signal, V_{CM} and interference from RF sources, V_{RF} and other biopotential signals within the body, V_{bio}. This understanding gives (5).

$$V_{in} = \{V_{EMG}, V_{CM}, V_{RF}, V_{bio}, V_{dc}\}. \quad (5)$$

The scope of this research does not include V_{RF} and V_{bio}. Consider the major interferences as V_{CM} and V_{dc}, which gives (6).

$$V_{out} = K[(V_{EMG1} + V_{CM1} + V_{dc1}) - (V_{EMG2} + V_{CM2} + V_{dc2})] \quad (6)$$

However, in reality, V_{CM} and V_{dc} measured at P_1 and P_2 are rarely identical. The phase and amplitude of V_{CM} can vary slightly across different points of the body due to skin impedance. V_{DC}, on the other hand, is dependent on the electrode contact pressure and variance of the half-cell electrolyte itself. Therefore, some baseline noise is always present at the output since the input signals V_{in1} and V_{in2} were never identical in the first place.

INPUT FILTER EVALUATION

Next, the three simple input filters are considered. Figure 3 (a) shows the EMG amplifier connected directly to the electrode. With no filter, the output V_{out} is prone to error due to DC offset. Figure 3 (b) is a simple filter, but the CMRR depends on the component tolerance, and CMRR can degrade due to the potential voltage divider (Huhta & Webster, 1973).

Figure 3 (c) is a design by Spinelli (2003). This design has a high CMRR but still requires the RLD. An improved design in Figure 3 (d) proposed by Wang (2013) does not require the RLD. This procedure aims to determine the V_{RLD} vs ΔV_{in} of the INA with the filters in place, as against unfiltered results from Figure 3.8(a). The procedure was performed by repeating the procedures with the filters in Figure 3.8 in place. All filters were set up to have a corner frequency of 0.156Hz.

The practical application of the four circuit designs was tested with actual muscle contraction. Two Ag-Cl electrodes, E1 and E2 were placed over the flexor digitorum superficialis muscle (FDS) and a third electrode, E3 was switched between the direct grounding and the RLD circuit, as shown in Figure 4. The electrodes were connected to the instrumentation amplifier with a shielded cable of 1.5m in length.

Readings were taken from the INA output, V_{out}, the common-mode voltage tapped from the gain resistors output, V_G and the RLD output, V_{RLD}. When the subject flexed the forearm, the FDS muscle output was acquired. The output of $V_{out\ was}$ recorded, and the EMG signal versus baseline noise was compared across the different filters and not using the filter at all. The procedure is repeated for all the designs in Figure 3. All filters were configured to have the same roll-off frequency. With C = 1 mF and R = 10MOhm, the roll-off frequency is 0.156 Hz.

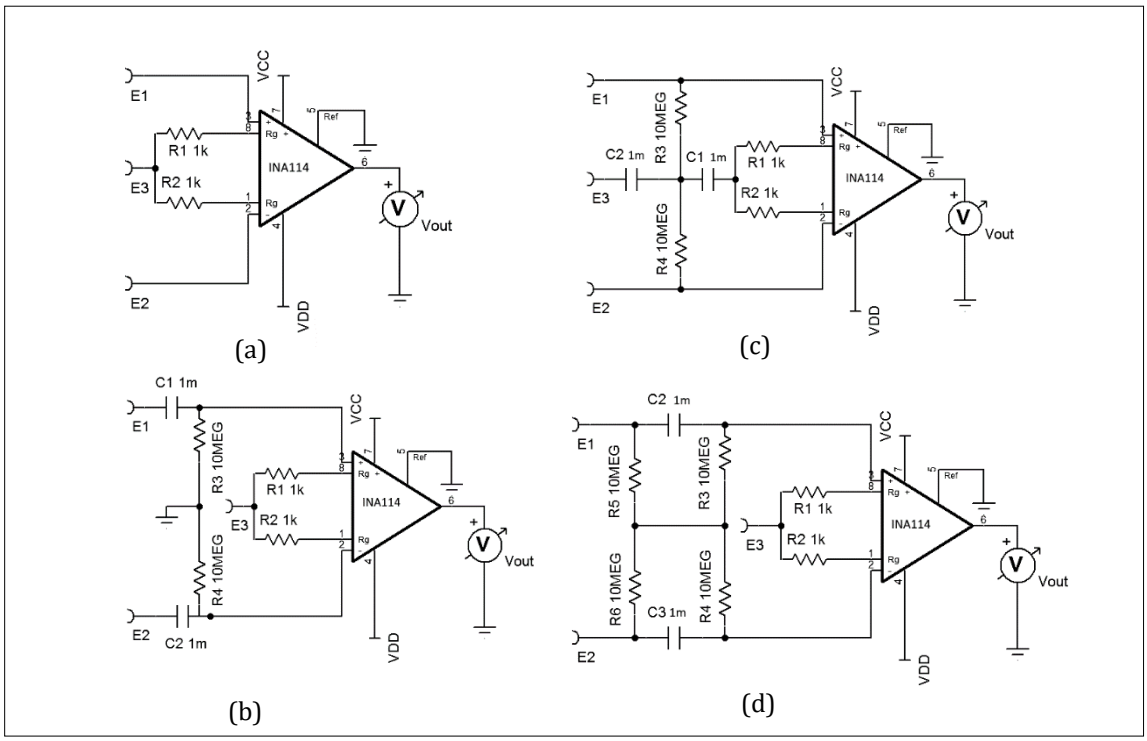

Figure 3. Input filter under test for DC rejection. (a) Direct input coupling, (b) standard RC filter, (c) design by Wang (2013) and (d) design by Spinelli (2003)

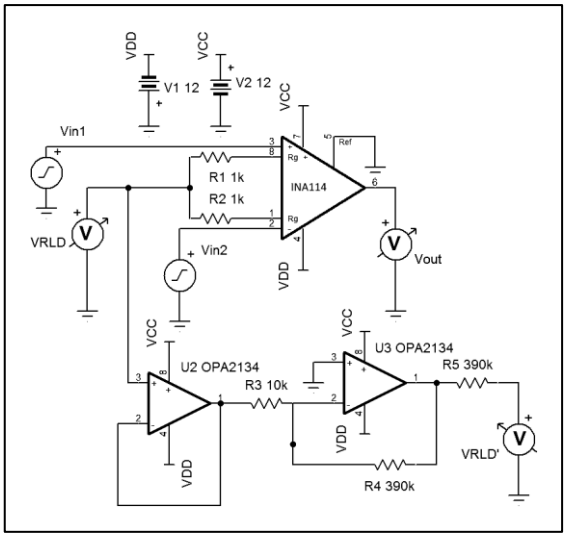

Figure 4. General Setup for measuring default DC offset. Vin1 and Vin2 were connected to a DC voltage supply and varied between -0.25 V to 0.25 V. The grounding can be grounded or switched to RLD.

INPUT IMPEDANCE, CMRR SIMULATION AND COMPARISON TO COMMERCIAL DEVICE

In differential amplifier design, a high input impedance and common-mode rejection ratio (CMRR) are important to ensure the signal is amplified correctly. The input impedance must be high to prevent signal attenuation and distortion. Modern instrumentation amplifiers have input impedance in the MΩ to GΩrange TINA SPICE. The CMRR is defined as the logarithmic ratio of the differential gain, A_{dm} to the common mode gain A_{cm} given as (7).

$$CMRR = 20\log_{10}\frac{A_{dm}}{A_{cm}} \tag{7}$$

As a validation measure, the performance of the amplifier was compared to a commercial unit *Motion Labs Z03 EMG Preamplifier*. During the time of testing, the unit was in use for muscle load analysis (Burhan et al., 2017). To measure the CMRR, a 0.01 V, 50 Hz sin wave signal was connected to the input of the amplifier. In differential mode, one input was connected to the source while the other was grounded. In common mode, both inputs were connected to the source.

RESULTS AND DISCUSSION

Figure 5 shows the sample amplified output of the results of the various filter designs in this study. The absence of the input filter in Figure 5(a) shows a DC offset of -0.35 V. In addition, the application of the RLD feedback circuit resulted in a high-frequency oscillation which distorted the baseline signal. In Figure 5(b), the RC filter provided a better CMRR for both direct grounding and the RLD method, with the RLD providing only marginally better performance. In Figure 5(c), the filter design by Wang et al. (2013) shows an improvement in floor noise level compared to the RC filter. The result of using the design by Spinelli et al. (2013) is shown in Figure 5(d), where it must be used with the RLD. A summary of the noise levels is provided in Table 2. The direct grounding data of Spinelli's design is not available as it can only work reliably with the RLD. As a result, the design by Wang (2013) was selected because it provided the lowest baseline noise and did not require the RLD circuit.

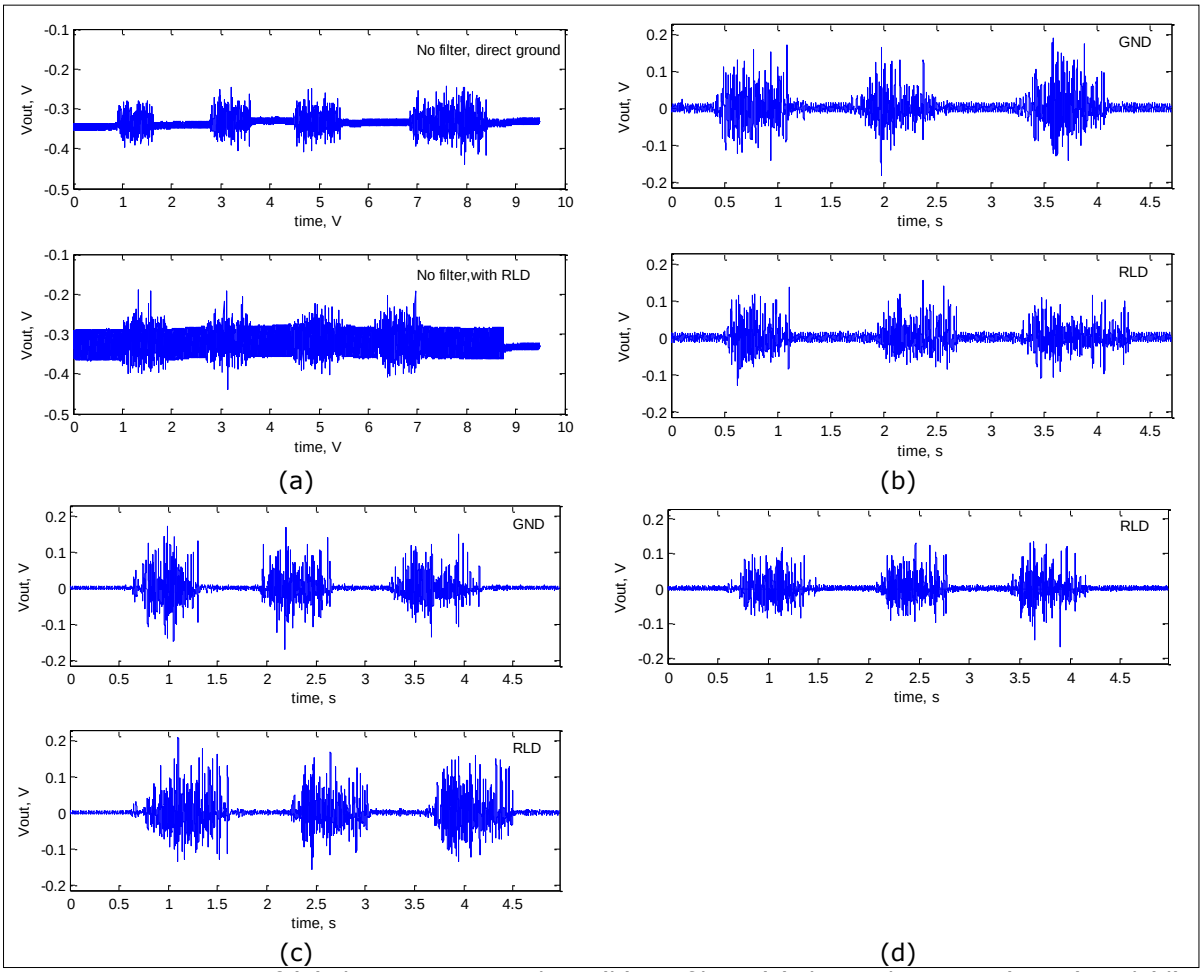

Fig. 5: Comparison of (a) direct input coupling, (b) RC filter, (c) design by Wang (2013) and (d) Spinelli (2013) without input filter for (top) direct ground method and (bottom) RLD

Table 2: Summary of the output signal of the compared filters

Filter type	V_{pp} (V)		V_{avg}(V)		V_{rms}(V)	
	GND	RLD	GND	RLD	GND	RLD
No filter	0.016	0.05	-0.35	-0.35	0.3202	0.3417
RC	0.022	0.022	0.001	0.001	0.64	0.065
Wang	0.01	0.01	0.001	0.001	0.031	0.033
Spinelli	N/A	0.01	0.001	0.001	N/A	0.031

Apart from direct input coupling shown in Figure 5(a), the baseline noise amplitude is similar between the RLD method and direct grounding. As for the case of the filter design of Wang et al. (2013), the result obtained in this study is consistent with their study.

To eliminate DC offset, front-end input filters can be used. The application of these filters can effectively reject DC offset and also improve the CMRR of the amplifier. Of the three filters in this study, the filter designed by Wang et al. (2013) produced the most favourable performance. This design is also preferred for future work due to its ability to work without the RLD.

Next, in EMG acquisition, the direct grounding method provided satisfactory noise suppression. The added complexity attributed to the RLD circuit did not provide a significant advantage. Furthermore, the RLD circuit requires careful implementation; in this experiment setup, the shock could be felt occasionally at the RLD electrode when it was driven to saturation due to DC offset. The reason for the shocks was not

investigated as it is beyond the scope of this research. The direct grounding method will remain as the design for the final circuit.

INPUT IMPEDANCE, CMRR AND COMPARISON TO COMMERCIAL DEVICE

The simulated input impedance of the designed amplifier in Figure 6 (a) shows the expected trend of the design. The differential mode input impedance is constant at 20 MΩ, with a gradual drop beyond 10 kHz. On the other hand, the common-mode impedance peaks at 20GΩ, in agreement with (C. S. Wang, 2013). Although in direct comparison these results are not as high as the rated specifications of the instrumentation amplifier, the application of the filter provides regulation towards DC offset and noise. In Figure 6 (b), the CMRR of the amplifier with the filter can reach above 120 dB. Although it is lower than the rating from the INA129 datasheet (130dB), it is important to note that CMRR also degrades from unbalanced input impedance. Thus, this design allows for a balanced impedance even if the components are not symmetrically matched.

Practical measurement and comparison to the Motion Labs Z03 were performed to rate the CMRR and general performance, as shown in Table 3. Figure 7 shows the physical comparison between the two amplifiers. For comparison purposes, the gain of the proposed design was adjusted to match the gain of the Z03, which is 300. The Z03 amplifier was attached with a propriety cable. Thus, the signal measurement was taken at the end connector of the cable. For the Z03, the rated CMRR is above 100 dB; however, the practical measurement was 96.34 dB. Similarly, the rated CMRR based on the INA129 is 120 dB, while the measurement was 93.36 dB. In this setup, the rated CMRR was not achievable due to a few reasons: first, the signal was produced by a single source function generator, and crocodile clips and breadboard jumpers were used to connect between the source amplifier under test and data acquisition unit. While all efforts were taken to ensure cables and components were spaced equally, it was difficult to ensure the occurrence of impedance or capacitive coupling at the connections.

However, using the Z03 amplifier as a reference, the difference between the measured CMRR of the proposed design is not far behind (-3dB). A comparison of recordings shown in Figure 8 shows the raw signal recording for both devices. The baseline noise is measured at 0.03 V_{RMS}, similar in both devices. The baseline noise is negligible; however, in the sample recordings, some apparent noise post-offset was due to residual EMG activity from the muscles.

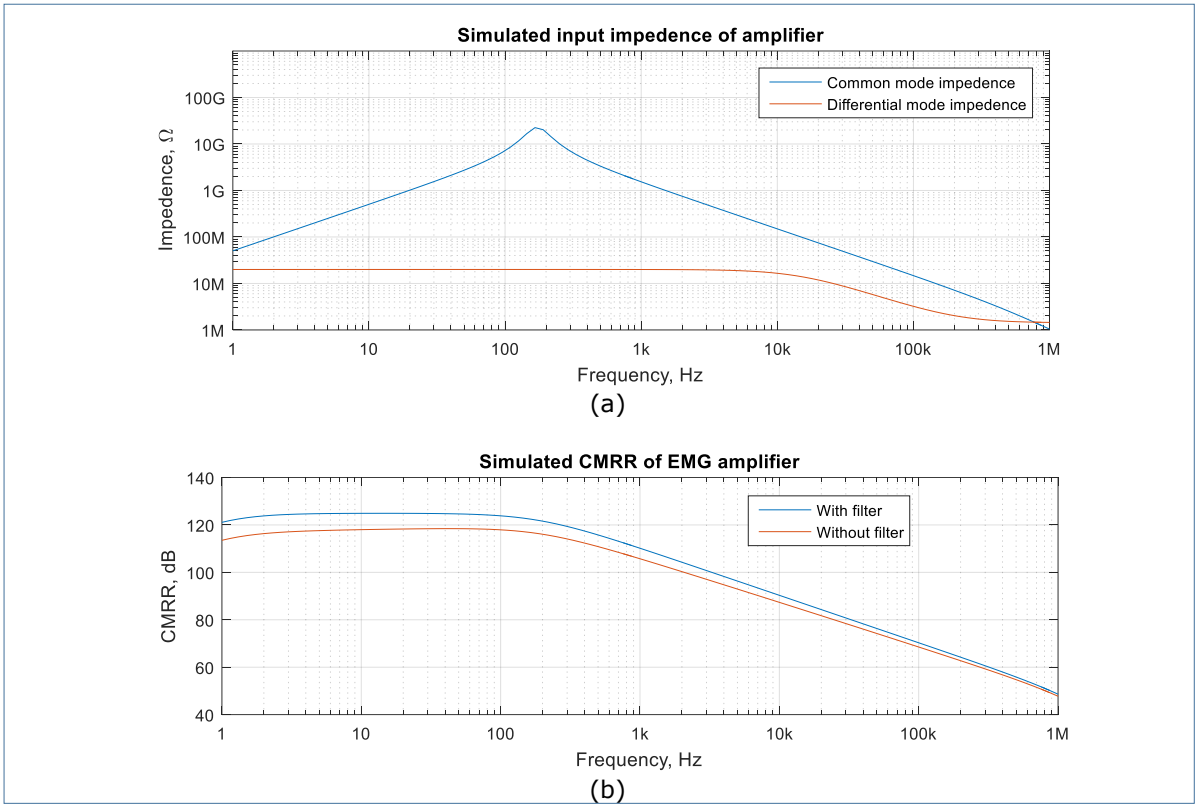

Figure 6. Simulated input impedance (a) and (b) CMRR of the proposed EMG amplifier design

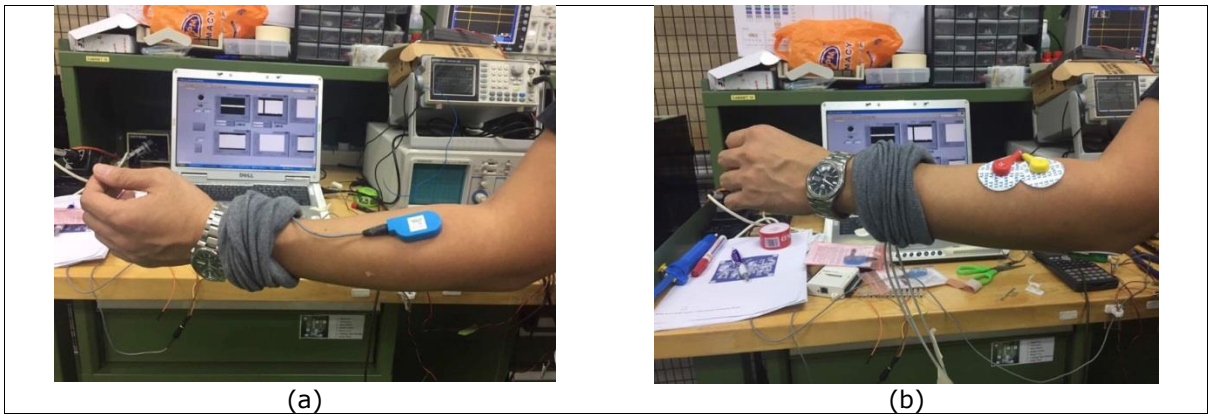

Figure 7. Comparison between (a) Motion Labs Z03 and (b) the proposed design

Table 3. Results of CMRR measurement

		Motion Lab Z03	This design (INA129P)	
			With filter	Without filter
Rated CMRR		>100dB	120dB (50 Hz, 100 x)	
Measured CMRR	Direct coupling	96.34	93.36	79.85
	With a 1.5m ECG cable	N/A	92.14	78.64
Rated input impedance		>100MΩ	>20GΩ, 150Hz (common-mode) 20MΩ (differential mode)	

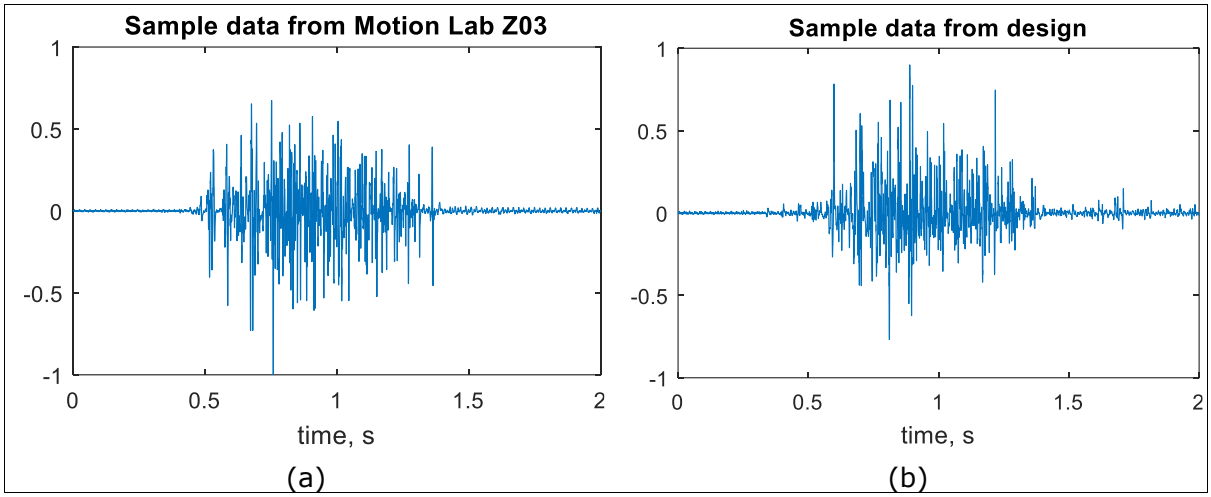

Figure 8. Comparison between the output of (a) Motion Lab Z03 and (b) the proposed design

CIRCUIT FABRICATION

The final circuit includes two non-inverting amplifiers to provide variable gain for the raw output and the linear envelope output. The CNC-milled circuit board of a single channel is shown in Figure 9(a). The design provides the flexibility of two outputs: a linear envelope and raw EMG. The circuit also features a two-gang power supply that facilitates connection to multiple boards. In Figure 9(b), the battery pack consisting of eight 18650 batteries (3.7 V lithium-ion) is connected to a voltage regulator followed by an over-current protection circuit and housed in an electronic casing.

The voltage regulator also functions as a voltage divider to provide the dual-voltage power supply to the op-amps. Figure 9(c) shows the internal arrangement of the six EMG amplifiers and their wiring. The completed device was connected to the battery pack as shown in Figure 9(d). The device is mobile and can be taken to any location easily. The electrodes are connected to the DB-15 connector, while the amplified analogue output is connected to the 4 mm banana plug outputs. The resulting cost of the amplifier was calculated at RM200 per channel. In addition, the amplifier draws 0.01 A of current when supplied with 12 V. This low power consumption is ideal for mobile applications.

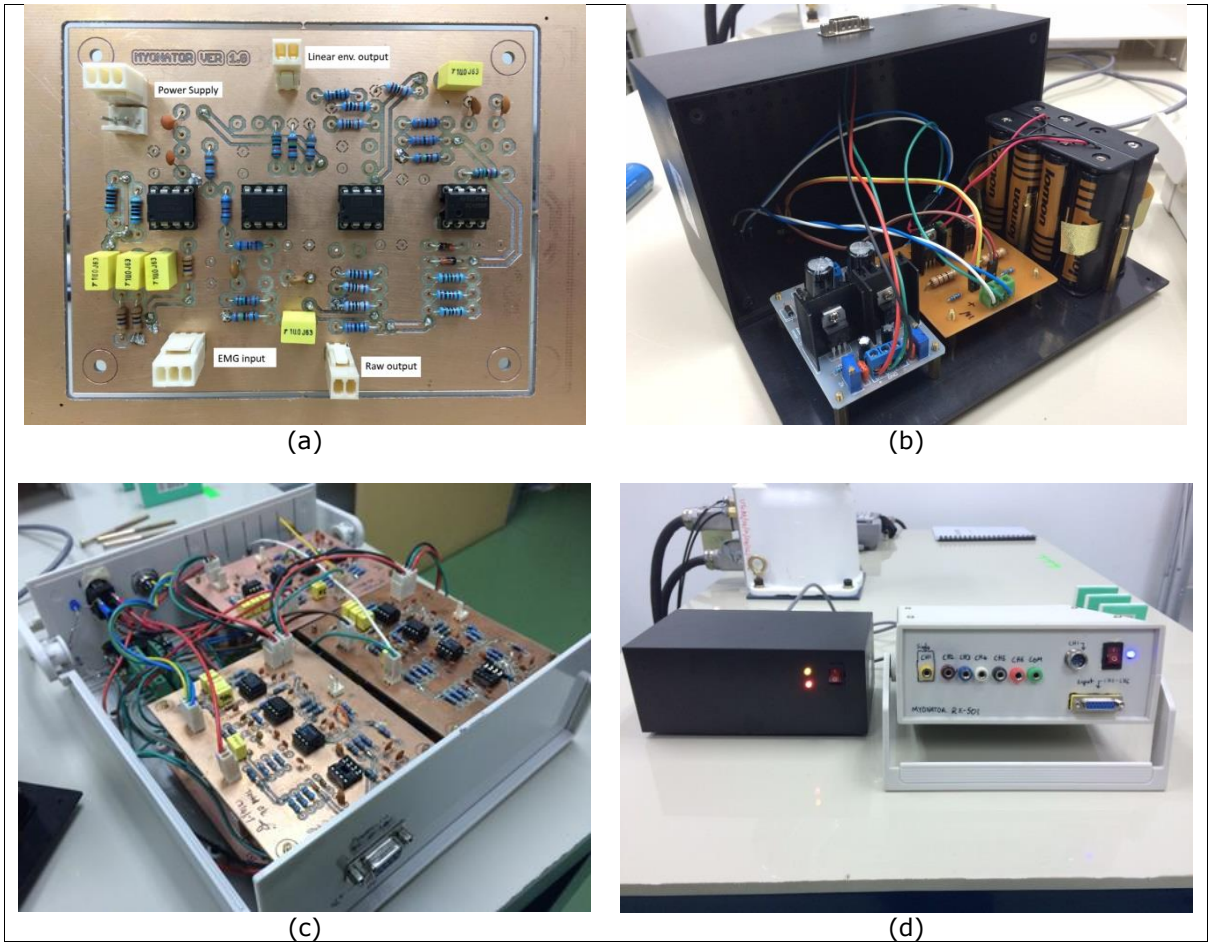

Figure 9: The EMG amplifier was developed in-house, (a) PCB, (b) power supply with short circuit protection, (c) assembly into the enclosure, (d) completed and functional equipment

CONCLUSION AND RECOMMENDATION FOR FUTURE WORK

In this work, we have shown proposed an EMG amplifier and validated its performance by physical measurement and comparison with a commercial device. Therefore, it can be concluded that the required performance from an EMG amplifier can be achieved at a low cost. For future works, the circuit can be further miniaturized by using surface-mount (SMD) components. The addition of an analogue-digital conversion (ADC) would eliminate the reliance on external acquisition devices.

References

Ajoudani, A., Tsagarakis, N., & Bicchi, A. (2012). Tele-impedance: Teleoperation with impedance regulation using a body-machine interface. *International Journal of Robotics Research*, *31*(13), 1642–1655. https://doi.org/10.1177/0278364912464668

Alnasser, E. (2014). The stability analysis of a biopotential measurement system equipped with driven-right-leg and shield-driver circuits. *IEEE Transactions on Instrumentation and Measurement*, *63*(7), 1731–1738. https://doi.org/10.1109/TIM.2013.2293811

Artemiadis, P. (2012). EMG-based Robot Control Interfaces: Past, Present and Future. *Advances in Robotics & Automation*, *01*(02), 10–12. https://doi.org/10.4172/2168-9695.1000e107

Avila, E. R., Junker, E., & Disselhorst-Klug, C. (2020). Introduction of an sEMG sensor system for autonomous use by inexperienced users. *Sensors (Switzerland)*, *20*(24), 1–17. https://doi.org/10.3390/s20247348

Benatti, S., Casamassima, F., Milosevic, B., Farella, E., Schönle, P., Fateh, S., Burger, T., Huang, Q., & Benini, L. (2015). A Versatile Embedded Platform for EMG Acquisition and Gesture Recognition. *IEEE Transactions on Biomedical Circuits and Systems*, *9*(5), 620–630. https://doi.org/10.1109/TBCAS.2015.2476555

Burhan, N., Kasno, M. A., Ghazali, R., Said, M. R., Abdullah, S. S., & Jali, M. H. (2017). Analysis of the Biceps Brachii Muscle by Varying the Arm Movement Level and Load Resistance Band. *Journal of Healthcare Engineering*, *2017*. https://doi.org/10.1155/2017/1631384

Hargrove, L. J., Simon, A. M., Young, A. J., Lipschutz, R. D., Finucane, S. B., Smith, D. G., & Kuiken, T. a. (2013). Robotic leg control with EMG decoding in an amputee with nerve transfers. *The New England Journal of Medicine*, *369*(13), 1237–1242. https://doi.org/10.1056/NEJMoa1300126

Huhta, J. C., & Webster, J. G. (1973). 60-Hz Interference in Electrocardiography. *IEEE Transactions on Biomedical Engineering*, *BME-20*(2), 91–101. https://doi.org/10.1109/TBME.1973.324169

Jones, M. (2015). Comparing DC Offset and Impedance Readings in the Assessment of Electrode Connection Quality. *NeuroRegulation*, *2*(1), 29–36. https://doi.org/10.15540/nr.2.1.29

Kim, D.-H., Lu, N., Ma, R., Kim, Y.-S., Kim, R.-H., Wang, S., Wu, J., Won, S. M., Tao, H., Islam, A., Yu, K. J., Kim, T., Chowdhury, R., Ying, M., Xu, L., Li, M., Chung, H.-J., Keum, H., McCormick, M., … Rogers, J. A. (2011). Epidermal electronics. *Science*, *333*(September), 838–843. https://doi.org/10.1126/science.1206157

Malboubi, M., Razzazi, F., & Aliyari, M. (2010). Elimination of Power Line Noise from EMG Signals Using an Efficient Adaptive Laguerre Filter. *International Conference on Signals and Electronic Systems*, *1*(2), 49–52.

Meattini, R., Benatti, S., Scarcia, U., De Gregorio, D., Benini, L., & Melchiorri, C. (2018). An sEMG-Based Human-Robot Interface for Robotic Hands Using Machine Learning and Synergies. *IEEE Transactions on Components, Packaging and Manufacturing Technology*, *8*(7), 1149–1158. https://doi.org/10.1109/TCPMT.2018.2799987

Northrop, R. B. (2001). *Noninvasive Instrumentation and Measurement in Medical Diagnosis*. CRC Press.

Park, K., Dankowicz, H., & Hsiao-Wecksler, E. T. (2012). Characterization of spatiotemporally complex gait patterns using cross-correlation signatures. *Gait and Posture*, *36*(1), 120–126. https://doi.org/10.1016/j.gaitpost.2012.01.016

Rechy-Ramirez, E. J., & Hu, H. (2015). Bio-signal based control in assistive robots: a survey. *Digital Communications and Networks*, *1*(2), 85–101. https://doi.org/10.1016/j.dcan.2015.02.004

Spinelli, E. M., Pallàs-Areny, R., & Mayosky, M. A. (2003). AC-coupled front-end for biopotential measurements. *IEEE Transactions on Biomedical Engineering*, *50*(3), 391–395. https://doi.org/10.1109/TBME.2003.808826

Staudenmann, D., Kingma, I., Daffertshofer, A., Stegeman, D. F., & Van Dieën, J. H. (2006). Improving EMG-based muscle force estimation by using a high-density EMG grid and principal component analysis. *IEEE Transactions on Biomedical Engineering*, *53*(4), 712–719. https://doi.org/10.1109/TBME.2006.870246

Steffes, M. (2012). *Design Sallen-Key low-pass filters with G >1, to achieve lower output noise*. http://www.planetanalog.com/document.asp?doc_id=528304

Tomasini, M., Benatti, S., Milosevic, B., Farella, E., & Benini, L. (2016). Power Line Interference Removal for High-Quality Continuous Biosignal Monitoring with Low-Power Wearable Devices. *IEEE Sensors Journal*, *16*(10), 3887–3895. https://doi.org/10.1109/JSEN.2016.2536363

Wang, C. S. (2013). A new AC-coupled amplifier for portable ECG without reference electrode. *Computers and Electrical Engineering*, *39*(1), 141–149. https://doi.org/10.1016/j.compeleceng.2012.07.011

Wang, J., Tang, L., & Bronlund, J. E. (2013). Surface EMG Signal Amplification and Filtering. *International Journal of Computer Applications (0975 – 8887)*, *82*(November), 15–22. https://doi.org/10.5120/14079-2073

Yoo, H. J., Park, H. J., & Lee, B. (2019). Myoelectric signal classification of targeted muscles using dictionary learning. *Sensors (Switzerland)*, *19*(10). https://doi.org/10.3390/s19102370

Yung, M., & Wells, R. P. (2013). Changes in muscle geometry during forearm pronation and supination and their relationships to EMG cross-correlation measures. *Journal of Electromyography and Kinesiology*, *23*(3), 664–672. https://doi.org/10.1016/j.jelekin.2013.01.001

Zhang, Y., Chen, Y., Yu, H., Yang, X., Lu, W., & Liu, H. (2018). Wearing-independent hand gesture recognition method based on EMG armband. *Personal and Ubiquitous Computing*, *22*(3), 511–524. https://doi.org/10.1007/s00779-018-1152-3